Phase Transformations and Properties Evolution of Alumina-Based Refractory Castables Containing ZnO and SiO$_2$

Containing ZnO and SiO$_2$

D. S. Fini[a], C. L. C. de Mauro[a], B. P. Bezerra[a,b], A. P. Luz[a,b]* ⓘ

[a]*Universidade Federal de São Carlos, Departamento de Engenharia de Materiais, Rod. Washington Luiz, km 235, 13565-905, São Carlos, SP, Brasil.*
[b]*Universidade Federal de São Carlos, Programa de Pós-Graduação em Ciência e Engenharia de Materiais, São Carlos, SP, Brasil.*

Although most of the studies presented in the literature are focused on MgAl$_2$O$_4$ formation and its role on alumina-based refractories performance, ZnO has been reported as a promising spinel inducer. Aiming to investigate the influence of ZnAl$_2$O$_4$ (ZA) and MgAl$_2$O$_4$ (MA) generation on the properties of alumina-based castables, three vibratable compositions containing calcium aluminate cement or hydratable alumina as binders and 1 wt% of silica fume, were evaluated in this work. Flexural strength, apparent porosity, hot elastic modulus, corrosion cup-tests, thermodynamic simulations, were carried out to analyze the performance of such ceramics. The results indicated that ZnAl$_2$O$_4$ was mainly formed above 800 °C, favoring an earlier sintering of the samples. Besides that, the softening of the castables was observed above 1200 °C, which resulted in the elastic modulus decay of the samples during their first heating cycle due to the formation of SiO$_2$-rich liquid phase in the resulting microstructure. Cement-free samples obtained after calcination (600 °C for 5h) presented enhanced corrosion resistance when placed in contact with molten slag at 1500°C. Although, silica fume addition to the castables negatively affected their corrosion performance, it helped to counterbalance the expansion associated with the spinel and calcium aluminates formation.

Keywords: *Alumina, ZnAl$_2$O$_4$, refractory castable, corrosion.*

1. Introduction

The search for solutions to improve productivity and minimize costs and environmental impacts has motivated various efforts in the refractory field to improve the performance of these ceramics. In this sense, spinel-containing products have received special attention due to their outstanding set of physical and chemical properties, including high refractoriness and resistance to chemical attack[1-3]. The most usual spinel phases incorporated into refractory compositions are those containing iron, magnesium, aluminum, and chromium (FeFe$_2$O$_4$, FeAl$_2$O$_4$, MgFe$_2$O$_4$, MgAl$_2$O$_4$, MgCr$_2$O$_4$). However, due to the carcinogenic nature of Cr^{6+}, environmental concerns have moved towards replacing chromium-containing refractories with less harmful alternative materials[2,4].

Although many investigations presented in the literature are focused on MgAl$_2$O$_4$ (MA) formation and its role on alumina-based refractories performance[2,5-7], ZnAl$_2$O$_4$ (ZA) or gahnite has been reported as a promising alternative, as this compound is non-toxic, harmless to nature and its formation can take place at lower temperatures than MA[8-12]. ZnAl$_2$O$_4$ formation takes place through the following mechanism: *(i)* a solid solution of zinc oxide in aluminum oxide is formed in the 600 °C to 700 °C temperature range, *(ii)* a disordered spinel structure is generated between 700 °C and 800 °C, and (iii) this structure is converted into

an ordered one at temperatures above 800 °C[11,12]. Therefore, such transformations may also favor an earlier sintering of the refractories, resulting in improved mechanical performance mainly above 800 °C[11].

Small contents of Zn(OH)$_2$ and basic zinc carbonate (0 to 0.66 wt%) added to high-alumina calcium aluminate cement-bonded castables can result in samples with higher flexural strength and lower susceptibility to crack generation and spalling, because ZA formation increases the number of sintering necks in the refractory matrix, improving ceramic bonding[11,13]. Additionally, this phase may affect the diffusion pathway between Al$_2$O$_3$ and CA (CaO.Al$_2$O$_3$) phase, hindering its reaction to form CA$_2$ (CaO.2Al$_2$O$_3$) and, subsequently, CA$_6$ (CaO.6Al$_2$O$_3$) grains at higher temperatures, thereby slightly reducing the permanent linear change (PLC) of the samples at 1550 °C[11,13].

However, the *in situ* generation of MgAl$_2$O$_4$ and calcium aluminates in refractories is accompanied with a large volume expansion (e.g., up to 8.4 vol% for MgAl$_2$O$_4$ formation)[10,14,15]. As pointed out by some authors[11,13,16,17], ZA generation in small amounts in alumina-based castables gives rise to micropores, whereas functionally optimum quantities of 21 wt% create undesirable expansion and porosity, increasing vulnerability to slag infiltration. Knowing that Zn^{2+} diffusivity is much higher than Al^{3+}, ZA formation will take place mainly by a one-way migration of ZnO (or Zn^{2+} ions) to Al$_2$O$_3$ creating an extreme scenario of Kirkendall effect[18,19]. This phenomenon can lead

to pores formation mainly along the $ZnO-ZnAl_2O_4$ interface, in contrast to MA spinel formation in which pores are found on both sides of the $MgO-Al_2O_3$ junction[17-20]. Hence, the microstructure disruption during $ZnAl_2O_4$ generation is more intense than $MgAl_2O_4$ formation, creating longer diffusion paths for ions/atoms and negatively affecting the mechanical properties of the castables.

Silica fume is another important component usually found in the matrix composition of spinel-containing castables. For MA-based refractories, SiO_2 is known to counterbalance the volumetric expansion associated with the spinel formation, by the generation of low-melting point phases in $Al_2O_3-CaO-SiO_2$ system, such as anorthite (CaO. $Al_2O_3.2SiO_2$ or CAS_2) and gehlenite ($2CaO.Al_2O_3.SiO_2$ or C_2AS)[21]. Knowing that the eutectic temperature of ZnO with SiO_2 is 1432 °C[19], which should favor liquid phase sintering and affect the mechanical properties of the refractories at high temperature, this paper investigated the role of silica fume in high alumina ZnO-containing castables and aimed to highlight the importance of the phase transformations understanding to design refractory castables with better performance.

2. Experimental

2.1. Evaluated compositions and their processing steps

Vibratable alumina-based castables containing ZnO and silica fume were designed considering the Alfred's particle packing model and distribution coefficient (q) equal to 0.26[22]. Tabular alumina ($α-Al_2O_3$ aggregates, d < 6 mm, Almatis, Germany), reactive and calcined aluminas [$α-Al_2O_3$, CL370 with specific surface area (SSA) = 3.0 m²/g, and CT3000SG with SSA = 7.2 m²/g, both from Almatis, Germany], magnesium oxide (dead-burnt, $α-MgO$, M30-B, d < 212 µm, SSA = 1.1 m²/g, RHI-Magnesita, Brazil), zinc oxide (analytical reagent grade, ZnO, d < 20 µm, SSA = 2.8 m²/g, LabSynth, Brazil) and silica fume (971U, amorphous SiO_2, Elkem, Norway) were selected as raw materials. The addition of 6 wt.% of hydratable alumina (HA, comprised mainly by θ and other metastable Al_2O_3 phases, Alphabond 300, SSA = 187 m²/g, Almatis, Germany) to AZAS and AZMAS (Table 1) as binder was analyzed, as the former composition would favor the $ZnAl_2O_4$ and mullite formation during the samples' thermal treatments, whereas the latter would induce the generation of $ZnAl_2O_4$, $MgAl_2O_4$ or even a complex spinel structure and silicates. AZCS composition, on the other hand, contained 6 wt.% of calcium aluminate cement (CAC, Secar 71, containing Al_2O_3 > 68.5 wt% and CaO < 31.0 wt%, SSA = 1.1 m²/g, Imerys Aluminates, France), which should favor the generation of $ZnAl_2O_4$, calcium aluminates and silica-containing phases in the castable's microstructure after firing. A fixed amount of zinc oxide or a mixture of zinc and magnesium oxides were selected to give rise to a total of approximately 21 wt% of spinel phases ($MgAl_2O_4$ and/or $ZnAl_2O_4$) in the evaluated compositions, which is similar to the previously reported formulations taken as reference[16].

The preparation of the designed compositions consisted of initially adding 0.2 wt% of a polyethylene glycol-based dispersant (Castament FS 60, Basf, Germany) to the dry-powders and then a dry and wet homogenization steps were carried out in a rheometer device[23]. It was stablished a standard mixing procedure, where the dry powders were stirred initially for 1 min (rotation speed = 20 rpm). After that, distilled water was gradually incorporated into the mixture and the wet mixing was carried out for approximately 3 min with 45 rpm. A final processing stage was also implemented, by applying high mixing rotating speed (~ 55 rpm) for 1 min to guarantee a suitable homogenization of the selected raw materials.

The water demand was adjusted to obtain mixtures with vibratable flow values around 150% (ASTM C 1445[24]). The molded samples were cured at 30 °C for 24 h and dried at 110 °C for another 24 h. The setting behavior of the fresh castables was also analyzed via ultrasonic measurements at room temperature (~ 23 °C) for 24 h, using the UltraTest device, IP-8 measuring system (Germany).

Aiming to identify the likely phases developed in the microstructure of the designed castables, simplified mixtures (comprising fine raw materials and better representing the matrix of the refractories, Table 2) were prepared and evaluated via X-ray diffraction measurements and thermodynamic calculations (with the help of FactSage software, version 6.4, CRCT (Canada) and GTT (Germany)). Firstly, the dry powders were mixed with distilled water (20 wt.%) for approximately 5 min at room temperature. The obtained suspensions were molded as cylindrical samples (30 mm x 30 mm) and kept at 30 °C for 24 h. After that, a drying step was conducted at 110 °C for another 24 h and the specimens were fired at 1000 °C, 1200 °C or 1500 °C with dwell time of 5 h and using heating rate of 1°C/min in a Lindberg Blue electric furnace. X-ray diffraction tests of the ground samples were carried out using D8 Focus equipment (Bruker, Karlsruhe, Germany) and with CuKα radiation [λ = 1.5418 Å], nickel filter, 40 mA, 40 mV, 2θ = 4° - 80° and scanning step = 0.02°.

Table 1. General aspects of the castables evaluated in this work.

Raw materials (wt. %)	AZAS	AZMAS	AZCS
Tabular alumina (d < 6 mm)	79.6	81.3	79.6
Calcined alumina (CL370)	2.0	2.0	1.0
Reactive alumina (CT3000SG)	2.0	2.0	3.0
Dead-burnt magnesia (d < 212 µm)	-	3.0	-
Zinc oxide (d < 20 µm)	9.4	4.7	9.4
Calcium aluminate cement (Secar 71)	-	-	6.0
Hydratable alumina (Alphabond 300)	6.0	6.0	-
Silica fume (971U)	1.0	1.0	1.0

Table 2. Matrix (d < 200 µm) components of the castable's compositions.

Raw materials (wt. %)	AZAS	AZMAS	AZCS
Tabular alumina (d < 200 µm)	44.9	49.5	44.9
Calcined alumina (CL370)	8.1	8.1	5.4
Reactive alumina (CT3000SG)	2.7	2.7	5.4
Calcium aluminate cement (Secar 71)	-	-	16.2
Magnesia (d < 212 µm)	-	8.1	-
Hydratable alumina (Alphabond 300)	16.2	16.2	-
Zinc oxide (d < 20 µm)	25.4	12.7	25.4
Silica fume (971U)	2.7	2.7	2.7

Table 3. Chemical composition of the selected synthetic slag.

Oxides (wt%)	SiO_2	TiO_2	Al_2O_3	Fe_2O_3	CaO	MgO	K_2O	SO_3	F
Slag	28.8	0.6	10.7	1.2	42.7	7.2	0.6	1.6	6.2

2.2. Characterization of the prepared castable samples

The influence of the phase transformations on the castables' elastic modulus (E) behavior was analyzed according to the ASTM C 1198-91[25] standard using the bar resonance technique (Scanelastic equipment, ATCP, Brazil. In such measurements, wide frequency scanning is performed to excite and capture the natural resonance frequencies of the castables. The elastic modulus is calculated based on the resulted vibration spectrum applying Pickett equations, which correlates the elastic modulus, the natural vibration frequencies, and the sample dimensions. For the fundamental flexural frequency of a rectangular bar, the Young's modulus is given by the following equation[26]:

$$E = 0.9465 \frac{mf_f^2}{b} x \frac{L^3}{t^3} x T_1 \qquad (1)$$

where, E is the Young's modulus (Pa), m the mass (g), b the width (mm), L the length (mm), t the thickness (mm), f_f the fundamental resonance frequency of the bar in flexure (Hz), and T_1 the correction factor for fundamental flexural mode to account for the finite thickness of the bar, Poisson's ratio, and others. Tests were carried out using dried (110 °C for 24h) bar samples (150 mm x 25 mm x 25 mm) in the 30 °C - 1400 °C temperature range with heating and cooling rates of 2 °C/min.

Permanent dimensional change (PLC, ASTM C113-14[27]) of bar samples (150 mm x 25 mm x 25 mm) was determined by measuring the specimens' length before and after firing at 800 °C, 1000 °C, 1200 °C and 1500 °C for 5 h. Cold mechanical strength measurements were carried out via 3-point bending tests (ASTM C133-97[28]) on cast prismatic castables' samples (150 mm x 25 mm x 25 mm) obtained after drying at 110 °C for 24h and firing at 800 °C, 1000 °C, 1200 °C and 1500 °C for 5 h and using a universal mechanical device (MTS-810, Material Test System, USA). The apparent porosity of such materials was also determined based on the procedure described by ASTM C830-00[29] and using kerosene as the immersion liquid. A total of five samples was analyzed for each selected condition and the presented values are the average result with their respective calculated standard deviation.

Corrosion cup tests were conducted with cylindrical samples (with an external d = 50 mm, h = 50 mm and a central inner role with 20 mm in diameter and 25 mm deep), which were divided into two groups (calcined and pre-fired ones, as they were heated up to 600 °C and 1500 °C for 5 h, respectively). During the tests, the inner cup of the castables were filled in with 8 g of synthetic slag and the set (refractory + slag powder) was placed in an electrical furnace and heated up to 1500 °C for 2 h under a heating rate of 2 °C/min. A total of 3 samples were analyzed for each studied condition and the chemical composition of the selected slag is shown in Table 3.

Table 4. Water demand and vibratable flow obtained for the evaluated castables.

Compositions	Water content (wt%)	Vibratable flow (%)
AZAS	5.0	149
AZMAS	5.2	156
AZCS	4.4	159

After cooling, the corroded samples were cut and had their cross sections observed using the Image J 1.42q software (Wayne Rasband, National Institutes of Health, USA) for the determination of the relative infiltrated area of the castable, as described in[30]. Additionally, thermodynamic calculations were carried out to predict the phases that should be formed during the initial slag-castable interaction, in the equilibrium condition at 1500 °C, using the FactSage software (version 6.4, databases = FactPS and FToxid, and the Equilib calculation modulus). The employed procedure consisted of firstly reacting 100g of slag with 100g of the castable and the resulting liquid was then considered as input in the following calculation step, when it was reacted again with more 100g of the castable. The simulations were carried out successively until the slag saturation was reached[31].

3. Results and Discussion

3.1. Flowability and curing behavior

Table 4 presents the water demand and flowability of the evaluated compositions during their processing steps. AZAS and AZMAS castables required higher liquid content (5.0-5.2 wt.%) during their preparation when compared with the cement (CAC)-bonded material (AZCS), which is explained by the high specific surface area (187 m²/g) and reactivity of the selected binder (hydratable alumina)[32]. Besides that, 8.3 up to 10% of additional water were incorporated into the mixtures containing 1wt.% of silica fume to obtain vibratable flow values close to the ones measured for the equivalent silica-free formulations[16].

Ultrasonic measurements were carried out at room temperature (~ 23 °C) to analyze the setting and curing behavior of the samples. Figure 1 compares the results obtained for the refractory compositions with (AZAS, AZMAS and AZCS) and without (AZA, AZMA and AZC) silica fume. The hydratable alumina-bonded castables presented faster hardening, as depicted by the increase of the ultrasonic wave propagation velocity detected after 2 hours. Although the cement-bonded compositions (AZC and AZCS) presented a slower setting (velocity increase around 4-10 h) in the evaluated conditions, the greater velocity values measured after 24 h of curing indicate that such material should present better green mechanical strength levels.

Regarding the role of silica in the setting behavior of the castables, this oxide is one of the most applied anti-hydration additives in MgO-containing castables due to its low cost and

Table 5. Predicted phases (wt%, obtained via thermodynamic simulations) generated in the matrix composition of the designed castables.

Compositions	Temperature (°C)	α-Al$_2$O$_3$	Na$_2$Ca$_3$Al$_{16}$O$_{28}$	NaAlSi$_3$O$_8$	Mg$_4$Al$_{10}$Si$_2$O$_{23}$	NaAlSiO$_4$	CaAl$_2$Si$_2$O$_8$	Ca$_2$AlSi$_2$O$_7$	CaAl$_{12}$O$_{19}$	Mullite	Liquid	Spinel (ss)
	1000	36.80	-	-	-	-	-	-	-	5.58	-	57.62
AZAS	1200	33.61	-		-	-	-	-	-	7.21	0.81	58.37
	1500	29.62	-	-	-	-	-	-	-	7.01	1.77	61.60
	1000	37.75	-	1.78	7.79	-	-	-	-	1.06	-	57.22
AZMAS	1200	34.21	-	-	-	-	-	-	-	6.65	1.54	57.61
	1500	28.28	-	-	-	-	-	-	-	6.13	2.21	63.38
	1000	28.51	3.21	-	-	-	0.73	10.35	-	-	-	57.21
AZCS	1200	-	-	-	-	1.23	3.40	3.04	34.20	-	-	58.13
	1500	-	-	-	-	-	-	-	27.33	-	14.18	58.49
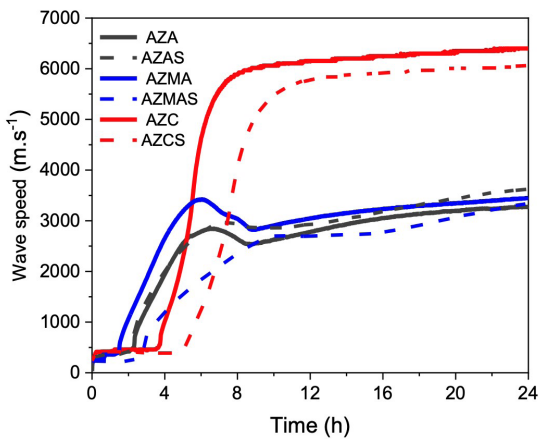
Figure 1. Curing behavior of the castables as a function of time at room temperature (~ 23 °C). AZA, AZMA and AZC results were previously presented by Pinto et al.[16].

Figure 2. In situ hot elastic modulus of the designed castables containing ZnO and 1 wt% of silica fume (AZAS, AZCS and AZMAS). Samples were cured at 30 °C for 24 h and dried at 110 °C for another 24 h before testing.

effectiveness[33-39]. In general, when amorphous and reactive silica is exposed to high alkaline environments (i.e., as the ones associated with MgO and calcium aluminate cement-containing compositions), it partially dissolves, leading to the formation of silicic acid. This acid can be attracted to the alkaline components, inducing the generation, for instance, of magnesium-silica-hydrated gels on the magnesia's surface[39,40]. Such phase transformations might limit the magnesia and CAC hydration, which explains the shift of the wave velocity increase to longer times, resulting in a delay of AZMAS and AZCS castable's setting (Figure 1). The distinct performance of the HA and CAC-bonded materials is directly related to the binders' reaction mechanisms and the hydrated phases (crystalline or gel-like compounds) formed in such materials[41,42].

3.2. Phase transformations as a function of the temperature

Figure 2 shows the elastic modulus (E) evolution of ZnO-containing compositions as a function of temperature during their first heating up to 1400 °C. Knowing that all compositions comprised hydraulic binders, heating the refractories above 110 °C led to the decomposition of the generated hydrates (i.e., aluminum hydroxides, magnesium

hydroxide, etc.,[41,42]) and, consequently, all E profiles presented a decay of the measured values mainly in the 200 °C - 800 °C temperature range [region (i)].

The CAC-bonded castable (AZCS) presented higher elastic modulus for all temperature ranges, pointing out that this binder resulted in better strengthening than HA. The beginning of the sintering process (with the increase of the samples' stiffness) could be identified mainly above 800 °C for all analyzed compositions, which can be related to the high Zn^{2+} mobility, favoring the formation of sintering necks and bridges at lower temperatures[11,13,19]. Besides that, E decay was noticed above 1200 °C mainly for AZAS and AZMAS castables [Figure 2, region (ii)] due to the formation of SiO$_2$-rich liquid phase in the samples' microstructure, as indicated in Table 5. Such behavior (softening at high temperature) was not detected for the equivalent silica-free compositions[16], which highlights the influence of this oxide in the thermomechanical performance of the refractories.

While cooling the castables, the previously formed liquid loses its mobility, resulting in a significant elastic modulus increase of the samples (Figure 2). Only AZCS castable showed E change (decrease) below 700 °C, pointing out

that a mismatch of thermal expansion coefficients among the distinct phases formed might have led to the samples' microcracking. The following sequence was obtained regarding the E values after the thermal treatment up to 1400 °C: 121 GPa (AZCS) > 102 GPa (AZMAS) > 80 GPa (AZAS).

Thermodynamic simulations were carried out to predict the phase transformations that should take place in the refractories structure at high temperatures (> 1000 °C). Table 5 indicates that all ZnO and MgO are expected to be consumed at 1000 °C, giving rise to spinel phase (which is a non-stoichiometric one) and its amounts varies around 57.22 to 63.38 wt.% in the evaluated temperature range.

The addition of silica fume to the compositions favors the formation of mullite ($Al_6Si_2O_{13}$), silica-containing compounds (i.e., $NaAlSi_3O_8$, $Mg_4Al_{10}Si_2O_{23}$, $NaAlSiO_4$, $CaAl_2Si_2O_8$ and $Ca_2AlSi_2O_7$) and liquid. The latter affected the elastic modulus evolution of the castables (Figure 2), and AZCS composition should contain the highest amount of this phase at 1500 °C (14.8wt.%) when compared to the other analyzed formulations. Besides that, all alumina should be consumed for the formation of $NaAlSiO_4$, $CaAl_2Si_2O_8$ and $Ca_2AlSi_2O_7$, $CaAl_{12}O_{19}$ (CA_6) and spinel (ss) in AZCS in the 1000-1500 °C range.

Although CA_6 generation was predicted to take place at 1000 °C by the simulations, the X-ray diffraction results indicated that such a phase is only formed at higher temperatures (Figure 3). The experimental data pointed out that corundum (α-alumina), $Na_2Al_{22}O_{34}$ (β-alumina), ZnO and $ZnAl_2O_4$ spinel (generated *in situ*) could be identified in AZAS and AZCS compositions after firing at 1000 °C. Moreover, CA ($CaAl_2O_4$ – derived from the CAC addition) and periclase (MgO) was still detected in AZCS and AZMAS samples, respectively, at this temperature, pointing out the need of higher thermal energy levels to induce CA_6 and $MgAl_2O_4$ formation in the selected time frame (5 hours) applied during the thermal treatments.

The calculated Gibbs free energy for $ZnAl_2O_4$ (ZA) and $MgAl_2O_4$ (MA) formation (-36.61 kJ/mol and -31.49 kJ/mol, respectively) confirms the greater likelihood of the former reaction product to be found in the designed compositions at 1000 °C, whereas magnesium aluminate spinel generation becomes more favorable when increasing the temperature (ZA = -33.33 kJ/mol and MA = – 35.43 kJ/mol at 1500 °C). The lack of MA in AZMA samples fired at 1000 °C indicates that the evaluated castables did not reach the equilibrium as predicted by FactSage™ and, to achieve this condition, the prepared samples should be kept at higher temperatures for longer times to allow all phase transformations to be completed.

All ZnO was consumed for $ZnAl_2O_4$ formation when firing the samples at 1200 °C (Figure 3). However, unreacted MgO was still present in AZMAS, indicating that a complete $MgAl_2O_4$ formation was not accomplished at 1200 °C. Alumina is the limiting reagent in the AZCS matrix fraction and, when considering the overall refractory composition (comprised by aggregates and fine components), it is expected that the remaining CA phase should also react with the coarse tabular alumina particles to generate mainly CA_2, CA_6 and the other silica-containing phases predicted by the thermodynamic calculations at 1200 °C. Moreover, it is reported that ZA formation might inhibit the diffusion pathway between Al_2O_3 and CA, hindering its reaction to form CA_2 and, subsequently, plate-shaped CA_6 grains[13].

Raising the firing temperature from 1200 °C to 1500 °C did not result in significant changes in AZAS phase composition (Figure 3). However, AZMAS still presented corundum, $ZnAl_2O_4$ and $MgAl_2O_4$ phases and small peaks of β-alumina and periclase (P) in its composition at 1500 °C. On the other hand, corundum consumption was identified for AZCS, giving rise to $CaAl_{12}O_{19}$ (CA_6) and gehlenite ($Ca_2AlSi_2O_7$).

Some differences in the identified phases via XRD (Figure 3) could be observed when comparing to the results
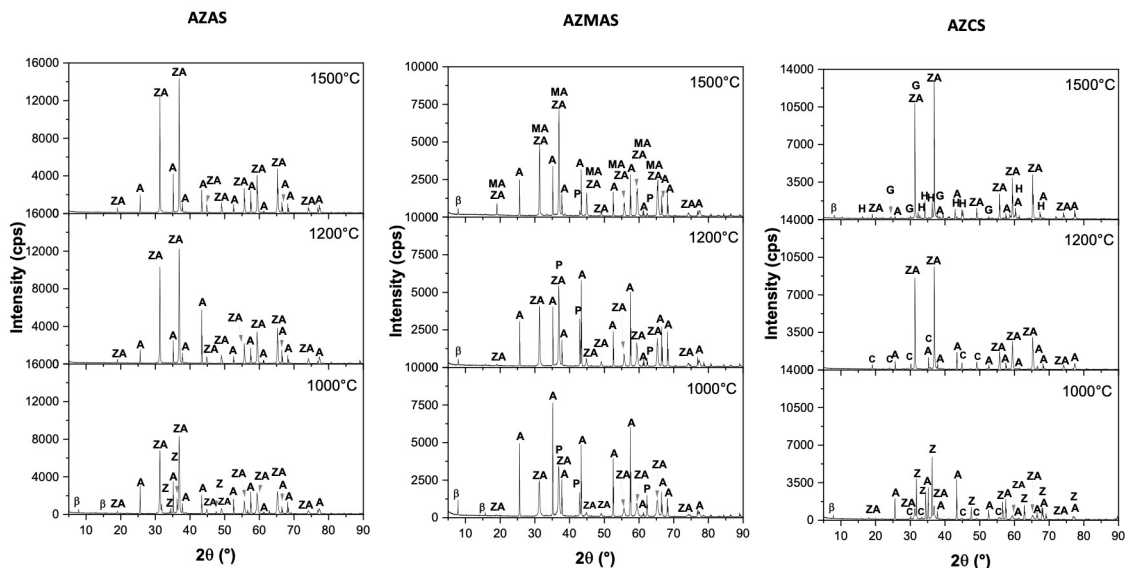
Figure 3. XRD profiles of the matrix samples (d < 200 μm) of the evaluated castables after firing at 1000, 1200 and 1500°C for 5h. XRD JCPDS cards: A (α-Al_2O_3) = 78-2426; β ($Na_2Al_{22}O_{34}$) = 31-7263; Z (ZnO) = 79-206; ZA ($ZnAl_2O_4$) = 74-1136; P (MgO) = 87-651; MA ($MgAl_2O_4$) = 75-1798; C ($CaAl_2O_4$ = 70-134); H ($CaAl_{12}O_{19}$) = 84-1613; G ($Ca_2AlSi_2O_7$) = 79-1725.

predicted by the thermodynamic calculations (Table 5), which is related to the fact that the latter represents a thermochemical equilibrium condition without taking into consideration the physical aspects of the raw materials (their particle size, scattering in the resulting microstructure, etc.), that influence the reactions rate at the selected temperatures.

These microstructural changes may also explain the properties evolution of the designed castables (aggregates + matrix fraction, Table 1). The permanent linear change (PLC, Figure 4a) was analyzed after heating and cooling bar samples at different temperatures to infer the dimensional stability of the refractories. AZAS samples expanded after thermal treatments between 800 °C and 1200 °C (reaching values ranging from 0.04% up to 0.67%), but the sintering and densification of the microstructure led to the shrinkage (-0.027%) of the pieces fired at 1500 °C. Branson[12] reported that $ZnAl_2O_4$ formation takes place in a one-way transference of ZnO through Al_2O_3. The quick unidimensional diffusion of ZnO may result in the samples expansion due to the Kirkendall effect[18,19]. Such a transformation may explain the increase in the linear dimension of AZAS samples from 800-1200 °C. Nevertheless, Borges et al.[17] also highlighted

that the formation of $MgAl_2O_4$ induces an expansion of ~ 8.4 vol%, whereas for $ZnAl_2O_4$ a shrinkage of ~ 0.25 vol% is expected. Consequently, adding ZnO instead of MgO as a spinel inducer tends to result in a lower overall expansion of the castables after firing at high temperatures.

AZCS refractory showed shrinkage of the pieces when firing them at 800 °C and an increase in their linear dimension could be detected up to 1500 °C, reaching PLC values around 0.92% (Figure 4a). $ZnAl_2O_4$ and calcium aluminates (CA, CA_2 and/or CA_6) generation is responsible for the greater expansion of this castable. On the other hand, a continuous increase of AZMAS samples linear dimension could be detected, which is associated to the formation of the spinel phases ($ZnAl_2O_4$ and $MgAl_2O_4$).

Table 6 points out the influence of silica in the dimensional stability of the refractories, comparing the PLC results obtained in this study with the ones collected for the equivalent silica-free castables[16]. As this additive leads to liquid generation at high temperature in the evaluated systems (Table 5), in general, this phase contributed to counterbalance the expansion associated with the spinel and calcium aluminates formation, reducing the overall expansion (negative values presented in Table 6) measured for the ZnO-containing refractories.
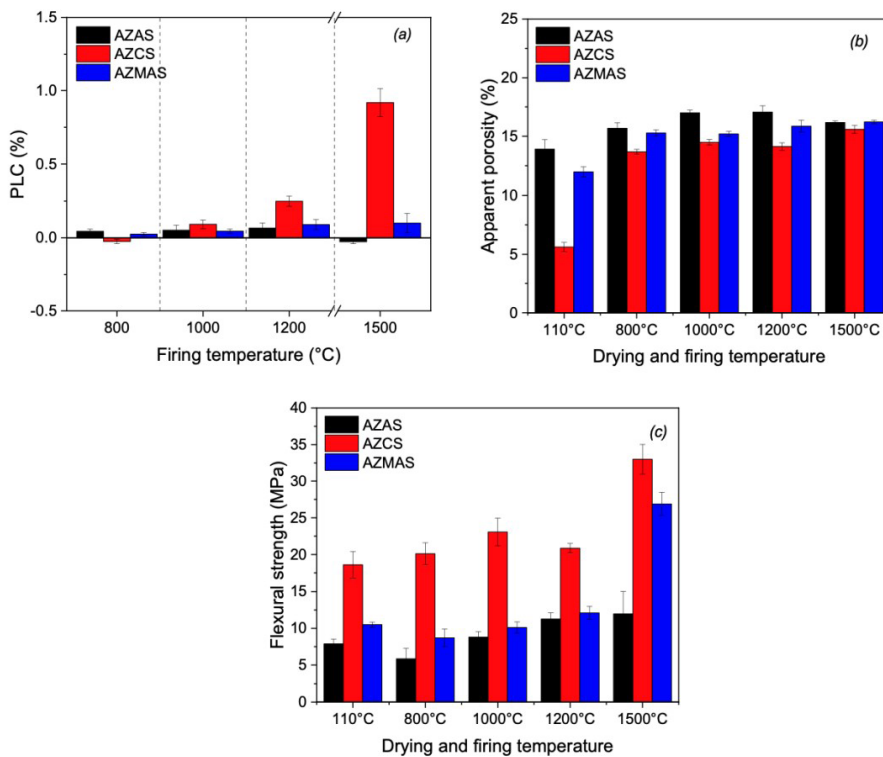
Figure 4. (a) Permanent linear change (PLC), (b) cold flexural strength and (c) apparent porosity of the dried and fired castable samples.

Table 6. Comparison of the permanent linear change (PLC) of the evaluated refractories with the silica-free castables presented by Pinto et al.[16].

Compositions	Difference between the PLC values obtained for the studied castables and the ones without SiO_2 addition			
	800°C/5h	1000°C/5h	1200°C/5h	1500°C/5h
AZAS	-0.023%	-0.232%	-0.251%	-0.157%
AZCS	+0.302%	+0.033%	-0.654%	+0.044%
AZMAS	+0.087%	-0.005%	-0.008%	-0.301%

Figure 4b indicates that AZAS and AZMAS refractories presented higher porosity (from 13.9 to 17.1% and 12.0 to 15.9%, respectively) than AZCS (from 5.6 to 15.6%), which can be related to the higher water demand of these materials during their processing steps, Table 4, as well as the formation and further decomposition of the gel-like hydrated phases derived from the hydration of HA[41,42]. Although a significant Kirkendall effect is expected during ZA nucleation (which will create porosity), the expansive MgAl$_2$O$_4$ formation should also act as an additional mechanism to increase the volumetric pore content of AZMAS refractory. Therefore, even though similar porosity values were achieved for the compositions containing ZnO or ZnO+MgO after firing at 1500 °C, the distribution and morphology of the pores can vary significantly[17-20], affecting the mechanical properties, as pointed out in Fig. 4c.

The CAC-bonded samples (AZCS) presented higher cold mechanical resistance in all evaluated conditions, which is explained by the action of the cement in the development of a more efficient binding effect than hydratable alumina. The ZnAl$_2$O$_4$, CA, CA$_6$ and gehlenite formation (Fig. 3) in the microstructure of AZCS enhances the flexural strength of this material (Figure 4c), whereas spinel generation (both ZA and MA) is the main responsible for improving the mechanical behavior of AZMAS after firing at 1500 °C.

3.3. Corrosion and thermodynamic simulations

To analyze the influence of the *in situ* spinel formation on the corrosion resistance of the evaluated castables, cup-tests were carried out at 1500 °C for the calcined (660 °C for 5 h) and pre-fired (1500 °C for 5 h) samples. Figure 5 shows the calculated slag infiltrated area after measuring the samples' region where liquid penetration took place.

Except for the calcined AZMAS samples, all silica-containing compositions presented higher slag infiltration compared to the SiO$_2$-free refractories (Figure 5). As liquid should be formed in the matrix fraction of AZAS, AZCS and AZMAS at 1500 °C (as pointed out in Table 5), this phase may be incorporated by the slag, making easier the infiltration of the latter into the refractories' microstructure. In general, the pre-firing treatment of these samples also affected negatively their corrosion behavior (Figure 5b), leading to an increase in the measured slag infiltration area, when comparing them to the ones calcined at 600 °C for 5h. Considering the expansive generation of CA$_6$, MgAl$_2$O$_4$ and ZnAl$_2$O$_4$ and their effects (i.e., changes in samples dimension after the heating procedure, as shown in Figure 4a), most likely the molten slag was able to find more available paths that favored its penetration in a greater extended manner in the castable fired structure (Figure 5c).
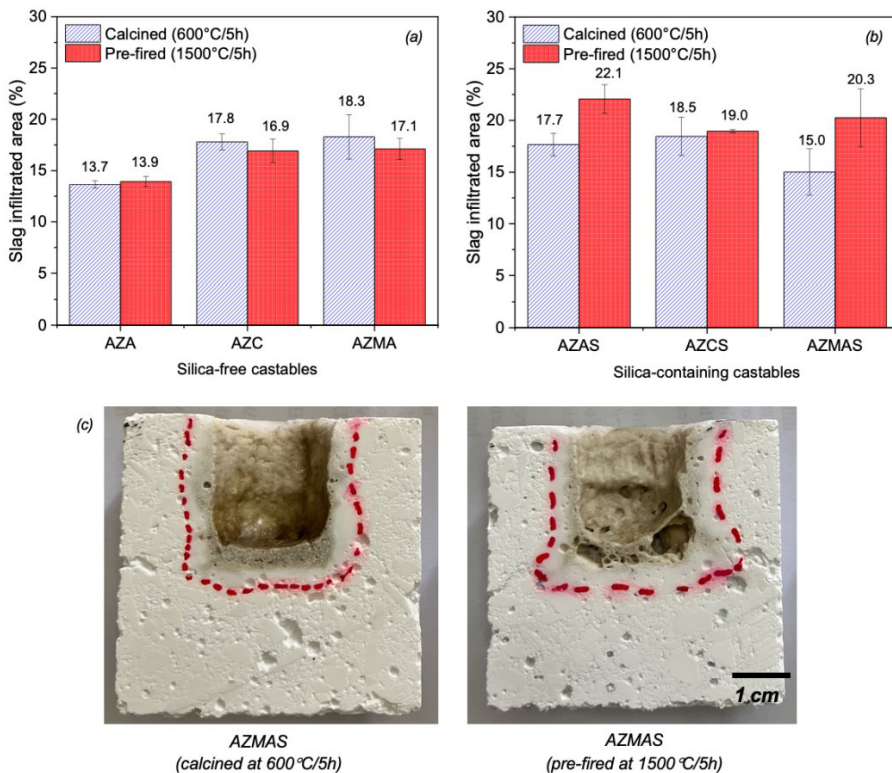
Figure 5. Slag infiltrated area when evaluating (a) silica-free (adapted from Pinto et al.[16]) or (b) silica-containing (1 wt.%) castables. The samples were calcined at 600 °C for 5h or fired at 1500 °C for 5 h before testing. The corrosion cup experiments were carried out at 1500 °C for 2 h. (c) Photographs of the calcined and pre-fired AZMAS samples after the corrosion tests. The red dashed lines point out the extent of the slag infiltration into the castables' microstructure.

Aiming to better understand the phase transformations during the corrosion tests of the refractories, thermodynamic simulations were also carried out to provide some insights on which phases should be dissolved / formed during the slag-refractory interaction at 1500 °C. Figure 6 indicates that as the slag reacts with the ZnO-containing castables, and the composition of the liquid changes up to its saturation, until the stage where the thermodynamic results show that the refractories should not be chemically further attacked by the slag.

A higher amount of resulting liquid (when compared to the silica-free compositions) was obtained after AZAS, AZCS and AZMAS interaction with the original molten slag. Corundum was consumed by reacting with CaO, derived from the liquid (Table 3), to give rise to $CaAl_{12}O_{19}$ (CA_6). Spinel ($ZnAl_2O_4$ and/or $MgAl_2O_4$) was the most resistance phase to the slag attack at 1500 °C, as it is not dissolved in the liquid formed with the selected slag. Besides that, the lower slag infiltration in the silica-free refractories

(Figure 5a) might be related to the greater amount of CA_2 and CA_6 phases precipitated in such systems (Figure 6). Previous studies[31,43] highlighted that tabular alumina aggregates may react with a high-CaO slag and generated calcium aluminate layers as an indirect dissolution product at the interface. These compacted layers act as a protective barrier against further infiltration, providing excellent slag corrosion indexes for the silica-free MgO-containing castables. Therefore, the same transformations are expected to take place in the ZnO-containing compositions presented here.

Few changes in the content of phases could be identified when comparing the thermodynamic results predicted for the AZAS and AZMAS castables (Figure 6), which indicates that from a chemical point of view, the compositions should present a similar corrosion behavior. However, other physical aspects are also important (i.e., samples' porosity, presence of cracks or flaws in the microstructure, etc.) as they influence the slag penetration rate and, consequently, the refractories' dissolution, as well as further precipitation of new phases.
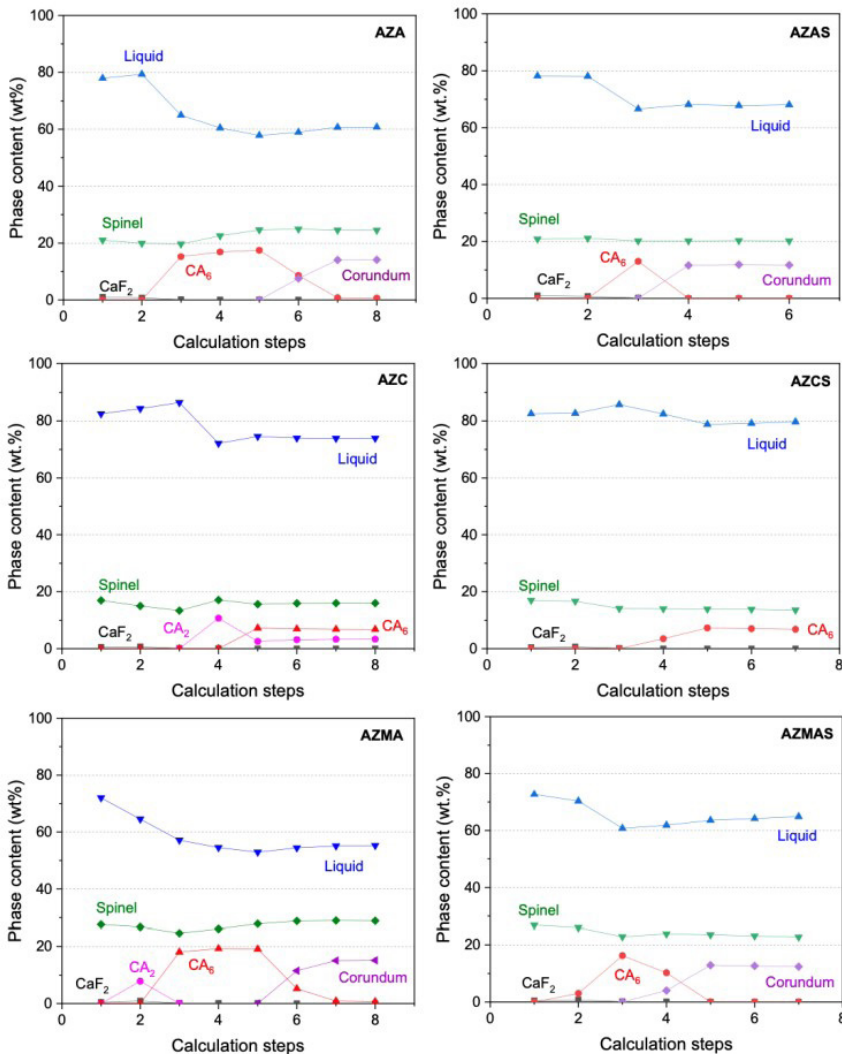
Figure 6. Predicted phases obtained via thermodynamic calculations for the interaction between the silica-free castables (AZA, AZC and AZMA) and the silica-containing ones (AZAS, AZCS and AZMAS) with a synthetic slag at 1500 °C and pressure = 1 atm.

Further microstructural analyses of the corroded samples (mainly the slag-refractory interface) are still required to better understand the distribution and morphology of the phases contained in such materials and such subjects should be explored in a forthcoming paper by the authors.

4. Conclusions

According to the obtained results, the binder (hydratable alumina or calcium aluminate cement) as well as the incorporation of silica fume into the evaluated compositions resulted in significant changes in the castables' rheology, physical and thermo-mechanical performance. Greater water content was required for the preparation of the SiO$_2$-containing mixtures when compared to silica-free equivalent refractories. Besides that, the presence of this oxide affected the magnesia and CAC hydration during curing step, shifting the setting time of AZMAS and AZCS castables to longer periods.

On the other hand, ZnAl$_2$O$_4$ generation was mainly identified above 800 °C, which favored an earlier sintering of the samples. Based on the hot elastic modulus measurements, a SiO$_2$-rich liquid phase was generated in the resulting microstructure of the castables above 1200°C and their softening could be identified during their first heating cycle. This aspect played an important role in the corrosion resistance of the refractories, as the formed liquid was incorporated by the slag during the corrosion experiments, making easier the infiltration of the latter into the solid structure. The generation of lower contents of calcium aluminate phases in the slag-refractory interface might also have an impact on the corrosion performance of the silica-containing compositions, as pointed out by the thermodynamic calculations.

Spinel phase proved to be an important component of the castables' microstructure, as it presents higher chemical stability (based on the thermodynamic simulations) when in contact with the selected slag at high temperatures. AZAS and AZMAS samples presented enhanced corrosion resistance when they were only calcined (600 °C for 5h) prior to the tests, which led to various phase transformations to take place in their microstructure along with the interaction of such refractories with the molten slag at 1500 °C. On the other hand, considering the expansive generation of CA$_6$, MgAl$_2$O$_4$ and ZnAl$_2$O$_4$, most likely the molten slag was able to find more available paths to infiltrate in the structure of the pre-fired samples during the corrosion tests. Further investigations are still required to better analyze the distribution of the formed phases and the interaction of the slag-refractory at the interface of the designed castables and this should be explored in a forthcoming paper by the present authors.

5. Acknowledgments

6. References

1. Fuhrer M, Hey A, Lee WE. Microstructural evolution in self-forming spinel;calcium aluminate castable refractories. J Eur Ceram Soc. 1998;18:813-20.

2. Zhang S, Lee WE. Spinel-containing refractories. In: Schacht CA, editor. Refractories handbook. UK: Taylor & Francis Inc.; 2004. p. 215-58.

3. Luz AP, Braulio MAL, Pandolfelli VC. Refractory castable engineering. Baden-Baden: Goller-Verlag; 2015. Spinel-containing alumina-based refractory castables; p. 497-592.

4. Goncharova MA, Karaseva OV, Maklakov SV, Bakhaev KV. Refractory materials for steel-making equipment lining. J Chem Technol Metall. 2018;53(5):924-8.

5. Mori J, Yoshimura M, Oguchi Y, Kawakami T. Effect of slag composition on wear of alumina-spinel castable for steel ladle. Taikabutsu Overseas. 1992;12:40-5.

6. Tomba Martinez AG, Luz AP, Braulio MAL, Sako EY, Pandolfelli VC. Revisiting CA$_6$ formation in cement-bonded alumina-spinel refractory castables. J Eur Ceram Soc. 2017;37:5023-34.

7. Sako EY, Braulio MAL, Luz AP, Zinngrebe E, Pandolfelli VC. Slag resistance of Al$_2$O$_3$-MgO refractory castables in different environmental conditions. J Am Ceram Soc. 2013;96(10):3252-7.

8. Ghosh A, Das SK, Biswas JR, Tripathi HS, Banerjee G. The effect of ZnO addition on the densification and properties of magnesium aluminate spinel. Ceram Int. 2000;26:605-8.

9. Xu P, Wang H, Ren L, Tu B, Wang W, Fu Z. Theoretical study on composition-dependent properties of ZnO·nAl2O3 spinels. Part II: Mechanical and thermophysical. J Am Ceram Soc. 2021;104(12):6455-66. https://doi.org/10.1111/jace.17997.

10. Hong WS, De Jonghe LC, Yang X, Rahaman MN. Reaction sintering of ZnO-Al$_2$O$_3$. J Am Ceram Soc. 1995;78:3217-24.

11. Li Y, Guo L, Chen L, Ding D, Ye G. Effect of Zn(OH)$_2$ on properties of corundum based castables bonded with calcium aluminate cement. Ceram Int. 2021;47:57-63.

12. Branson DL. Knetics and mechanism of the reaction between zinc oxide and aluminum oxide. J Am Ceram Soc. 1965;48:591-5.

13. Guo L, Wang X, Li Y, Mu Y, Jia Q, Wang G, et al. Evolution in properties of high alumina castables containing basic zinc carbonate. Ceram Int. 2021;47(13):19019-25.

14. Leblud C, Anseau MR, Di Rupo E, Cambier F, Fierens P. Reaction sintering of ZnO-Al$_2$O$_3$ mixtures. J Mater Sci. 1981;16:539-44.

15. Nakagawa Z. Expansive behavior of powder compacts during spinel formation. Mass Charg Transp Ceram. 1996;283-94.

16. Pinto VS, Luz AP, Borges OH, Pandolfelli VC. Binder effect on ZnAl$_2$O$_4$-containing high alumina refractory castables. Ceram Int. 2022;48(8):11401-9.

17. Borges OH, Sardelli JAP, Pagliosa C, Luz AP, Pandolfelli VC. ZnO and MgO as inducers of spinel-like phase formation on alumina-based castables. J Eur Ceram Soc. 2022;42(15):7335-42.

18. Fan HJ, Knez M, Scholz R, Nielsch K, Pippel E, Hesse D, et al. Monocrystalline spinel nanotube fabrication based on the Kirkendall effect. Nat Mater. 2006;5:627-31.

19. Mandal S, Hemrick JG, Mahapatra MK. Zinc aluminate (ZnAl$_2$O$_4$) refractory aggregates: dilatometric sintering studies and thermal expansion coefficient. J Eur Ceram Soc. 2022;42:6244-54.

20. Okada H, Kawakami H, Hashiba M, Miura E, Nurishi Y, Hibino T. Effect of physical nature of powders and firing atmosphere on ZnAl$_2$O$_4$ formation. J Am Ceram Soc. 1985;68:58-63.

21. Sako EY, Braulio MAL, Milanez DH, Brant PO, Pandolfelli VC. Microsilica role in the CA$_6$ formation in cement-bonded spinel refractory castables. J Mater Process Technol. 2009;209(15–16):5552-7.

22. Dinger DR, Funk JE. Particle packing, part II: review of packing of polydisperse particle systems. InterCeram Int Ceram Rev. 1992;41(2):95-7.

23. Pileggi RG, Pandolfelli VC, Paiva AE, Gallo J. Novel rheometer for refractory castables. Am Ceram Soc Bull. 2000;79(1):54-8.

24. ASTM: American Society for Testing and Materials. ASTM C1445: standard test method for measuring consistency of castable refractory using a flow table. West Conshohocken: ASTM International; 2013.

25. ASTM: American Society for Testing and Materials. ASTM C1198-91: standard test method for dynamic young's modulus, shear modulus, and poisson's ratio for advanced ceramics by sonic ressonance. West Conshohocken: ASTM International; 2002.

26. Pickett G. Equations for computing elastic constants from flexural and torsional resonant frequencies of vibration of prisms and cylinders. In: Proceedings-American Society for Testing and Materials; 1945; Philadelphia. Proceedings. Philadelphia: American Society for Testing and Materials; 1945. p. 846-65.

27. ASTM: American Society for Testing and Materials. ASTM C113-14: standard test method for reheat change of refractory brick. West Conshohocken: ASTM International; 2019.

28. ASTM: American Society for Testing and Materials. ASTM C133-97: Standard test methods for cold crushing strength and modulus of rupture of refractories. West Conshohocken: ASTM International; 2015.

29. ASTM: American Society for Testing and Materials. ASTM C830-00: standard test methods for apparent porosity, liquid absorption, apparent specific gravity, and bulk density of refractory shapes by vacuum pressure. West Conshohocken: ASTM International; 2016.

30. Braulio MAL, Martinez AGT, Luz AP, Liebske C, Pandolfelli VC. Basic slag attack of spinel-containing refractory castables. Ceram Int. 2011;37(6):1935-45.

31. Luz AP, Braulio MAL, Tomba Martinez AG, Pandolfelli VC. Slag attack evaluation of in situ spinel-containing refractory castables via experimental tests and thermodynamic simulations. Ceram Int. 2012;38(2):1497-505.

32. Racher RP, Kockegey R, Buchel G, Buhr A, Gierisch D. Improvement in workability behavior of calcia-free hydratable alumina binders. In: Unitecr 2005; 2005; Orlando, USA. Proceedings. Orlando: The Metallurgy and Materials Society; 2005. p. 402-7.

33. Sandberg B, Myhre B, Holm JL. Castables in the system MgO-Al_2O_3-SiO_2. In: Unified International Technical Conference on Refractories; 1995; Kyoto. Proceedings. Ohio: American Ceramic Society; 1995. p. 3-11.

34. Hundere A, Myhre B, Odegard C, Sandberg B, Zhou N, Zhang S, et al. Magnesium-Silicate-Hydrate bonded MgO-Al_2O_3 castables. In: Annual Conference of Metallurgists; 1999; Quebec. Proceedings. Quebec: The Metallurgy and Materials Society; 1999. p. 2–7.

35. Bjorn M, Peng H, Ming L. Cement free MgO castables: part I: Flow, setting and slaking. Proc of UNITECR. 2013;2013:881-6.

36. Odegard C, Feldborg H, Myhre B. Magnesia-silica-hydrate bonded MgO castables. In: Unified International Technical Conference on Refractories (UNITECR 01); 2001; Cancun, Mexico; 2001. Proceedings. Cancun: American Ceramic Society. p. 1-10.

37. Sandberg B, Mosberg T. Use of microsilica in binder systems for ultralow cement castables and basic, cement-free castables. Ceram Trans. 1989;4:245-58.

38. Kalousek GL, Mui D. Studies on formation and recrystallization of intermediate reaction products in the system magnesia-silica-water. J Am Ceram Soc. 1954;37(2):38-41.

39. Salomão R, Pandolfelli VC. Microsilica addition as an anti-hydration technique for magnesia-containing refractory castables. Am Ceram Scoeity Bull. 2007;86(6):9301-6.

40. Souza TM, Luz AP, Santos T, Gimenes DC, Miglioli MM, Correa AM, et al. Phosphate chemical binder as an anti-hydration additive for Al_2O_3-MgO refractory castables. Ceram Int. 2014;40(1):1503-12.

41. Lee WE, Vieira W, Zhang S, Ahari KG, Sarpoolaky H, Parr C. Castable refractory concretes. Int Mater Rev. 2001; [cited 2022 sep 16];46(3):145-67. http://www.tandfonline.com/doi/full/10.1179/095066001101528439

42. Parr C, Auvray JM, Pelletier J, Szepizdyn M, Wohrmeyer C, Zetterstrom C. A review of refractory bond systems for monolithic castable refractories. In: Fiftieth Annual Symposium on Refractories; 2014; St Louis, USA; Proceedings. Ohio: American Ceramic Society; 2014. p. 18-35.

43. Sako EY, Braulio MAL, Pandolfelli VC. The corrosion resistance of microsilica-containing Al_2O_3–MgO and Al_2O_3–spinel castables. Ceram Int. 2012;38(6):4783-9.